Atomistic Modeling of Macromolecular Crowding Predicts Modest Increases in Protein Folding and Binding Stability

Sanbo Qin and Huan-Xiang Zhou*
Department of Physics and Institute of Molecular Biophysics, Florida State University, Tallahassee, Florida

ABSTRACT Theoretical models predict that macromolecular crowding can increase protein folding stability, but depending on details of the models (e.g., how the denatured state is represented), the level of stabilization predicted can be very different. In this study, we represented the native and denatured states atomistically, with conformations sampled from explicit-solvent molecular dynamics simulations at room temperature and high temperature, respectively. We then designed an efficient algorithm to calculate the allowed fraction, f, when the protein molecule is placed inside a box of crowders. That a fraction of placements of the protein molecule is disallowed because of volume exclusion by the crowders leads to an increase in chemical potential, given by $\Delta\mu = -k_BT \ln f$. The difference in $\Delta\mu$ between the native and denatured states predicts the effect of crowding on the folding free energy. Even when the crowders occupied 35% of the solution volume, the stabilization reached only 1.5 kcal/mol for cytochrome b_{562}. The modest stabilization predicted is consistent with experimental studies. Interestingly, a mixture of different sized crowders was found to exert a greater effect than the sum of the individual species of crowders. The stabilization of crowding on the binding stability of barnase and barstar, based on atomistic modeling of the proteins, was similarly modest. These findings have profound implications for macromolecular crowding inside cells.

INTRODUCTION

Inside cells, protein and RNA molecules occupy >30% of the volume (1). The crowded conditions are expected to have significant effects on biophysical properties of proteins. Thanks to concerted efforts based on theoretical modeling (2–7), atomistic simulations (8,9), and in vitro experiments (10–13), a qualitative understanding on the effects of macromolecular crowding on protein folding and binding stability has been reached. Crowders, because of excluded volume, raise the chemical potential of a test protein, and more so to the protein molecule when its conformation is more open (14). Thereby, crowding shifts the folding equilibrium toward the native state and the binding equilibrium toward the bound state. Here we report quantitative predictions of the effects of crowding on folding and binding stability based on atomistic modeling of protein molecules.

Simple theoretical models can be valuable in providing physical insight into how crowding may affect protein folding and binding. They are designed to capture the essential physics but lack realistic details. For examples, proteins in the native state have been modeled as spheres. Although theoretical models can be constructed to fit a specific set of experimental data, the predictive power of such models is questionable. In fact, the predicted levels of crowding-induced stabilization by different models can be significantly different (5,6). Therefore, quantitatively the value of simple theoretical models may be limited. This limitation was a main motivation for this approach of atomistic modeling.

Cheung et al. (8) and Stagg et al. (9) carried out Langevin dynamics simulations of the folding and unfolding of two different proteins, each represented by a coarse-grained C_α side-chain model, in the presence of spherical crowders. The simulations allowed them to calculate the changes in folding free energy by the crowders. Similarly, Minh et al. (15) carried out Brownian dynamics simulations of the flap motions of a protein, represented by a coarse-grained C_α-only model, in the presence of spherical crowders. The simulations showed that crowding shifts the equilibrium between open and closed conformations toward the latter.

In this study, we took a different approach to calculate the effects of crowding on thermodynamic properties. Instead of calculating the free-energy differences between two end states in the absence and presence of crowders, represented by the two horizontal legs in Fig. 1 *A* for protein folding and Fig. 1 *B* for protein binding, we calculated the transfer free energies of protein molecules from a dilute solution to a crowded solution, as represented by the vertical legs in Fig. 1, *A* and *B*. The change in folding free energy by crowding is (14)

$$\Delta\Delta G_f = \Delta\mu_N - \Delta\mu_D, \quad (1)$$

where $\Delta\mu_N$ and $\Delta\mu_D$, respectively, are the changes in chemical potential when a protein molecule in the native and denatured states are placed in a crowded solution. Similarly, the change in binding free energy of two proteins, A and B, by crowding is

$$\Delta\Delta G_b = \Delta\mu_C - (\Delta\mu_A + \Delta\mu_B), \quad (2)$$

where $\Delta\mu_A$, $\Delta\mu_B$, and $\Delta\mu_C$, respectively, are the changes in chemical potential when the two protein molecules and their complex are placed in a crowded solution.

Submitted February 2, 2009, and accepted for publication March 23, 2009.

*Correspondence: hzhou4@fsu.edu

Editor: Gerhard Hummer.

0006-3495/09/07/0012/8 $2.00

doi: 10.1016/j.bpj.2009.03.066

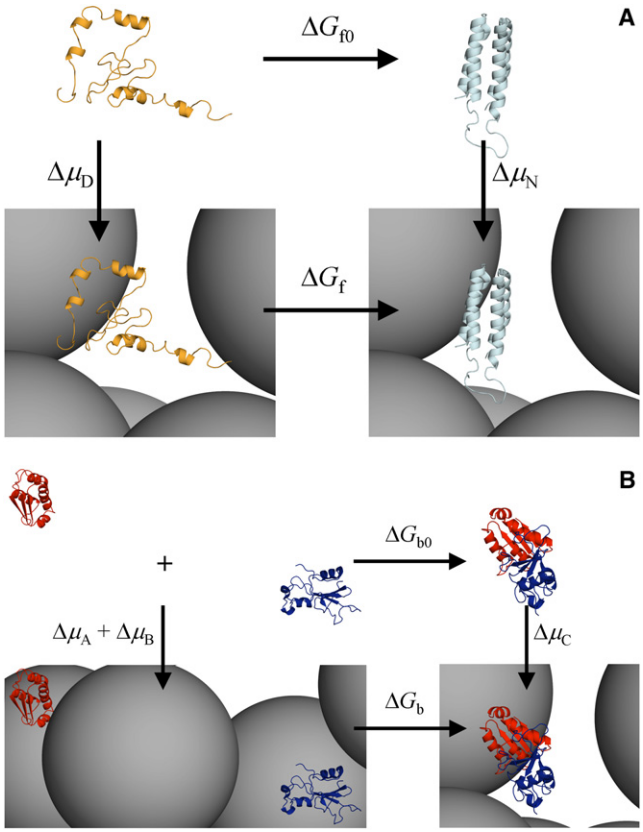

FIGURE 1 Thermodynamic cycles for calculating the effects of crowding on (*A*) folding free energy and (*B*) binding free energy. The horizontal legs are folding or binding free energies in the absence (ΔG_{f0} or ΔG_{b0}) and presence (ΔG_f or ΔG_b) of crowders; the vertical legs are the changes in chemical potential of the denatured or unbound state ($\Delta\mu_D$ or $\Delta\mu_A + \Delta\mu_B$) and native or bound state ($\Delta\mu_N$ or $\Delta\mu_C$). Orange and cyan ribbons show denatured and native cytochrome b_{562}, respectively; blue and red ribbons show barnase and barstar, respectively. Black spheres represent crowders.

The approach based on the vertical legs complements those based the horizontal legs. In particular, the crowding-induced changes in chemical potential of the end states (e.g., the native and denatured states in protein folding) yield valuable insight into the physical basis of crowding effects. In addition, the approach makes it possible to dissect the different contributing factors of crowding. In this study, we specifically focused on the volume exclusion of crowders. This volume exclusion precludes some of the placements when a protein molecule is introduced into a crowded solution, so that only a fraction, f, of all placements is allowed. The resulting change in chemical potential is given by

$$\Delta\mu = -k_B T \ln f, \tag{3}$$

where k_B is Boltzmann's constant and T is absolute temperature. Since $f < 1$, the change in chemical potential due to volume exclusion of crowders is always positive. Equation 3 can be seen as a specialization of Widom's insertion theorem (16) to hard particles.

Here we designed a very efficient algorithm for calculating the allowed fraction f of a test protein and applied it to study the effects of crowder volume exclusion on protein folding and binding stability. The approach has significant potential in other applications and in enabling more and more realistic modeling of cellular environments.

METHODS

In the overall design of our approach, the test protein in a dilute solution and a collection of crowders were independently simulated. Representative conformations (totaling M_p) of the test protein and representative configurations (totaling M_c) of the crowders were saved. The protein in each representative conformation was then tested against each representative configuration of the crowders to calculate a value for the allowed fraction f. The $M_p \times M_c$ such values were averaged to give the final value for f.

Below we describe the procedures for the simulations of the test proteins, the crowders, and the algorithm for calculating f.

Conformational sampling for cytochrome b_{562} in native and denatured states

Cytochrome b_{562} is a four-helix protein with 106 residues (Fig. 1 *A*). In a separate study to elucidate its unfolding mechanism, molecular dynamics simulations of this protein were carried out at 300 K and 500 K in explicit solvent (H. Tjong and H.-X. Zhou, unpublished), following protocols published in a similar study (17). The total lengths of the two trajectories were 30 ns and 15 ns, respectively. Here we sampled 1000 conformations each from the room temperature and high temperature trajectories to represent cytochrome b_{562} in the native and denatured states, respectively. (Note that the focus in this study is on the folding stability. The effects of crowding on folding intermediates such as the transition state will be presented in a further study (H. Tjong and H.-X. Zhou, unpublished)). The average radii of gyration in the two sets of conformations were 15.8 and 17.9 Å, respectively. Representative conformations of native and denatured cytochrome b_{562} are displayed in Fig. 1 *A*.

Conformational sampling for barnase and barstar in bound and unbound states

To represent the bound state of barnase and barstar, 548 conformations of their complex were sampled from a 7.2-ns trajectory generated in a previous study (18). Each of these conformations was then separated to yield the conformations of unbound barnase and barstar. A representative conformation of the barnase-barstar complex is displayed in Fig. 1 *B*.

Generation of configurations for crowders

In this study, the crowders were represented by spheres. We have previously used such a hard-sphere system to study the effects of crowding on protein binding kinetics (19). Following that study, we used the hard-sphere simulation program in the book of Allen and Tildesley (20) to generate configurations of crowders with the same size. Briefly, hard sphere were initially present at the sites of a face-centered cubic (FCC) lattice and randomly assigned velocities according to the Maxwell distribution. They moved with uniform velocity until elastic collision with other spheres. The periodic boundary condition and minimum-image convention were applied during the simulations. Snapshots were then saved as representative configurations of the crowders.

The primary simulation box was a cube with side length of 10^3 Å. For a desired crowder radius R_c and a desired crowder volume fraction ϕ, the number, N, of crowders was determined from $N(4\pi/3)R_c^3 = \phi \times 10^9$ Å^3. The total number of sites of an FCC lattice is given by $4n^3$, where n is an

integer. We chose the minimum n that satisfied $4n^3 \geq N$. From the $4n^3$ sites, N was randomly selected as initial positions for the crowders. Four crowder radii, at 15, 20, 30, and 50 Å, and four volume fractions, at 5%, 15%, 25%, and 35%, were studied. The 16 combinations of R_c and ϕ, the number of crowders in the simulation box for each combination, and the size of the FCC lattice used for initial positions of the crowders, are listed in Table 1.

For each combination of R_c and ϕ except for $R_c = 15$ Å and $\phi = 35\%$, a single simulation trajectory was initiated; 10 configurations of the crowders, separated by 10^6 collisions, were saved as representatives. The case $R_c = 15$ Å and $\phi = 35\%$ yielded the lowest value for the allowed fraction (see below) and hence had the greatest demand on calculation accuracy. In this case, we started 84 independent trajectories. After 1.5×10^7 collisions, the final configurations of the 84 trajectories were saved as representatives.

Mixtures of crowders with two different sizes, at 15 and 50 Å, were also studied. With the total volume fraction kept at 35%, the two types of crowders were mixed in 18 different proportions (see Table 2). Generating representative configurations for these mixtures required modifications of the procedure just described for crowders with the same size. In preparing the initial configuration for each mixture, two FCC lattices were used. One was for the 15 Å crowders and had 4×19^3 sites; the other was for the 50 Å crowders and had 4×6^3 sites. From the second lattice, the desired number of sites was randomly selected as initial positions of the 50 Å crowders. The first lattice was then superimposed onto the second, and all sites were eliminated where the placement of a 15 Å crowder would lead to overlap with the existing 50 Å crowders. Among the remaining sites in the first lattice, the desired number was randomly selected as initial positions of the 15 Å crowders. In the propagation of the mixed crowders, the Allen-Tildesley program was also modified to account for the different radii of the crowders. For each mixture, 10 representative configurations of the crowders, separated by 10^6 collisions, were saved.

Algorithm for calculating the fraction of allowed placements

In calculating the allowed fraction f, we treated the test protein molecule in each conformation and the crowders in each configuration as hard particles. The protein molecule was modeled as a collection of van der Waals spheres with Bondi radii (21). In principle, f can be calculated by randomly placing the protein molecule, with a given conformation, inside a given configuration of the crowders (the system was kept at constant volume). If out of P random placements, P_a placements were successful in that they do not lead to overlap between the test protein and the crowders, then $f = P_a/P$.

TABLE 1 Crowded solutions generated by crowders with a single size

R_c (Å)	ϕ (%)	N	$4n^3$
15	5	3537	$4 \times 10^3 = 4000$
15	15	10,610	$4 \times 14^3 = 10976$
15	25	17,684	$4 \times 17^3 = 19652$
15	35	24,757	$4 \times 19^3 = 27436$
20	5	1492	$4 \times 8^3 = 2048$
20	15	4476	$4 \times 11^3 = 5324$
20	25	7460	$4 \times 13^3 = 8788$
20	35	10,445	$4 \times 14^3 = 10976$
30	5	442	$4 \times 5^3 = 500$
30	15	1326	$4 \times 7^3 = 1372$
30	25	2210	$4 \times 9^3 = 2916$
30	35	3095	$4 \times 10^3 = 4000$
50	5	95	$4 \times 3^3 = 108$
50	15	286	$4 \times 5^3 = 500$
50	25	477	$4 \times 5^3 = 500$
50	35	668	$4 \times 6^3 = 864$

TABLE 2 Crowded solutions generated by mixed crowders with two sizes

ϕ_1 (%)	ϕ_2 (%)	N_1	N_2
35	0	24,757	0
31.5	3.5	22,281	66
28	7	19,805	133
24.5	10.5	17,330	200
21	14	14,854	267
17.5	17.5	12,378	334
14	21	9902	401
10.5	24.5	7427	467
7	28	4951	534
6.125	28.875	4332	551
5.25	29.75	3713	568
4.375	30.625	3094	584
3.5	31.5	2475	601
2.8	32.2	1980	614
1.75	33.25	1237	635
0.7	34.3	495	655
0.35	34.65	247	661
0	35	0	668

We developed a far more efficient algorithm for calculating the allowed fraction when a protein, represented with atomic details, is placed into a random distribution of crowders. The basic idea of the algorithm is to first expand each crowder to the largest distances at which the test protein can still overlap with the crowder and then calculate f as the fraction of space not filled by the expanded crowders (Fig. 2). In our calculation, the center of the test protein was placed on a three-dimensional grid (and the center of each crowder is moved to the nearest grid as an approximation). To find the required expansion of a crowder, the test protein was placed at grid points around the crowder. At each grid point, overlap between the test protein and the crowder was checked by calculating the distance between each protein atom and the crowder. The expansion was comprised of all the grid points that led to overlap. This part of the calculation was done only once and then by translation mapped to all the crowders in the simulation box. After the mapping, f was obtained by counting the number of grid points not covered by any expanded crowder. The value of f was then averaged over crowder configurations and over conformations of the test protein. Finally, the change in chemical potential by crowding was calculated by Eq. 3. For protein folding, the calculations were done separately for the native protein and for the denatured protein, yielding the effect of crowding on the folding stability (Eq. 1). Similarly, for protein binding, the calculations were done separately for the complex and for the two subunits, yielding the effect of crowding on the binding stability (Eq. 2).

Test of the algorithm

This algorithm was exhaustively tested. Because the test protein was placed on a grid, a sufficiently fine grid spacing must be used. To illustrate the effect of the grid spacing, in Fig. 3 we display the volume of the expanded crowder calculated at grid spacings from 0.14 to 3.0 Å. The relative error decreased to <0.1% as the grid spacing was reduced to 1.5 Å and further decreased to 0.01% at a grid spacing of 1 Å. We used a 1 Å grid spacing in all subsequently calculations.

By comparing the results for $\Delta\Delta G_f$ calculated on different configurations of the crowders, the calculation errors were found to be under 0.05 k_BT except for the case $R_c = 15$ Å and $\phi = 35\%$; in that case, the error was 0.2 k_BT.

The problem of placing a spherical test protein into a box of spherical crowders has an approximate analytical solution, provided by the scaled particle theory (SPT) (22). The theory, which has been used to model macromolecular crowding (2,3,5–7), predicts the allowed fraction according to

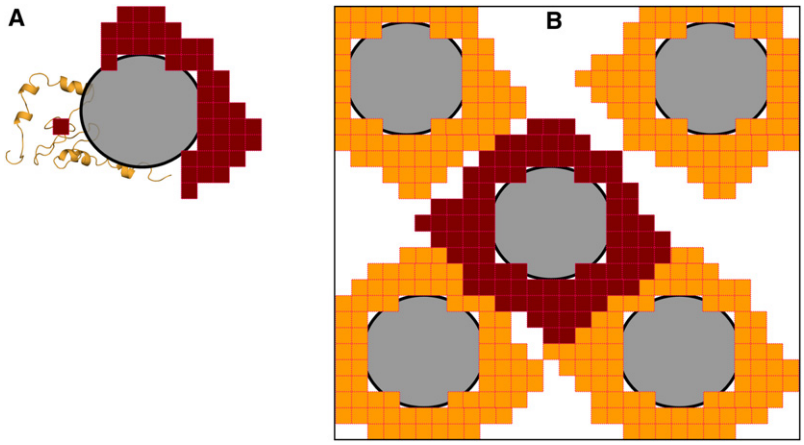

FIGURE 2 Illustration of the algorithm for calculating the allowed fraction. (*A*) The region around a crowder is filled by grids, each representing a location where the test protein will overlap with the crowder. (*B*) The filled region is mapped to each crowder in the simulation box. The total number of unfilled grids divided by the total number of grids in the box gives the allowed fraction.

$$-\ln f = \Delta\mu/k_BT = -\ln(1-\phi) + \frac{CS_c}{1-\phi}a + \left[\frac{CR_c}{1-\phi} + \frac{(CS_c)^2}{8\pi(1-\phi)^2}\right]S + \left[\frac{C}{1-\phi} + \frac{C^2R_cS_c}{(1-\phi)^2} + \frac{(CS_c)^3}{12\pi(1-\phi)^3}\right]V, \quad (4)$$

where a, S, and V are the radius, surface area, and volume, respectively, of the test protein, $S_c = 4\pi R_c^2$ is the surface area of the crowders, and C is their number density. For $a = 20$ Å and $R_c = 20$ Å, the f values obtained from our calculations were 0.644 ± 0.001, 0.194 ± 0.001, 0.0296 ± 0.0005, and 0.00130 ± 0.00009, respectively, at $\phi = 5\%$, 15%, 25%, and 35%. The values predicted by the SPT are 0.643, 0.192, 0.0283, and 0.00107, respectively. Overall, there is good agreement between calculation and theory, but there are systematic discrepancies at high ϕ-values. The discrepancies increase with decreasing R_c. We attributed the discrepancies to underestimation by the SPT. The severity of the approximation made in the SPT is known to increase both with increasing ϕ and with decreasing R_c.

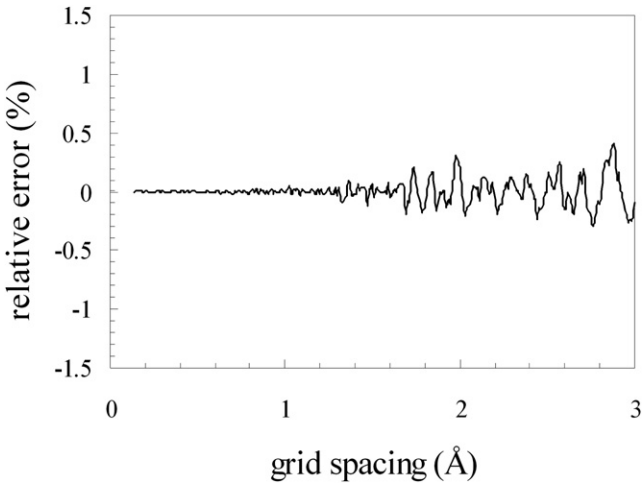

FIGURE 3 Effect of grid spacing on the calculated volume of an expanded crowder. The radius of the bare crowder was 15 Å. At a given grid spacing, the relative error was calculated by comparing the calculated volume against the exact result; the latter was taken as the average of the values calculated at six fine grid spacings: 0.14–0.19 Å with an increment of 0.01 Å.

RESULTS

Folding stability in the presence of a single species of crowders

The change in folding stability of cytochrome b_{562} by the addition of 85 g/L of PEG 20 K has been measured by Ai et al. (12). We calculated $\Delta\mu_N$ and $\Delta\mu_D$, the crowding-induced increases in chemical potential of this protein in the native and denatured states. The resulting change in the folding free energy is displayed in Fig. 4 for four crowder sizes (R_c from 15 to 50 Å) and four crowder volume fractions (ϕ from 5% to 35%). At a given crowder size, the level of stabilization increases with increasing volume fraction occupied by the crowders, consistent with expectation.

At a given crowder volume fraction, the level of stabilization decreases as the crowder size increases from 15 to 50 Å. This result can be understood as follows. Only a small number of large crowders is needed to produce the same volume fraction as a large number of small crowders. The small number of

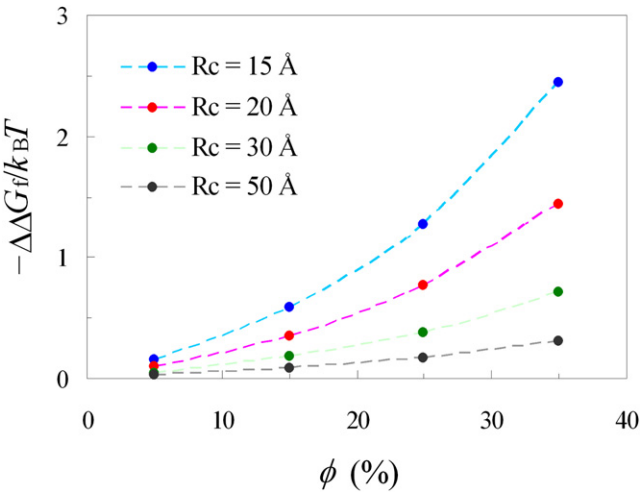

FIGURE 4 Dependence of $\Delta\Delta G_f$ on crowder radius R_c and volume fraction ϕ. Circles show calculated results; curves show results from fitting to Eq. 4.

large crowders leaves large voids in which the more open denatured state can be accommodated nearly as well as the compact native state, leading to a diminishing $\Delta\Delta G_f$. In contrast, a large number of small crowders would lead to small voids, which become much more discriminating against the more open denatured state, leading to a relatively large magnitude in $\Delta\Delta G_f$.

The dependences of $\Delta\mu_N$ and $\Delta\mu_D$ on R_c and ϕ can be fitted very well to Eq. 4 when a, S, and V were treated as adjustable parameters. The fitted values of these parameters were 20.6 Å, 5165 Å^2, and 16,569 Å^3, respectively, for native cytochrome b_{562} and 24.9 Å, 6873 Å^2, and 18,154 Å^3, respectively, for the denatured protein. Fig. 3 shows that the results for $\Delta\Delta G_f$ calculated from the fitting of $\Delta\mu_N$ and $\Delta\mu_D$ and from the actual values of $\Delta\mu_N$ and $\Delta\mu_D$ are indistinguishable.

Experimentally, Ai et al. (12) observed a level of stabilization at 0.4 k_BT by the addition of 85 g/L of PEG 20 K. In our atomistic modeling, this level of stabilization could be produced by crowders with a radius of 20 Å and occupying 15% of volume. The highest level obtained in our study, produced by crowders with a radius of 15 Å and occupying 35% of volume, was 2.5 k_BT, or 1.5 kcal/mol at room temperature.

Folding stability in the presence of mixed crowders

The cytosol is crowded by many species of macromolecules. To make progress toward mimicking cellular environments, we studied the effects of mixtures of crowders with two different sizes on folding stability. Crowders with radii of 15 and 50 Å were mixed to yield a fixed total volume fraction of 35%. Fig. 5 displays the results for $\Delta\Delta G_f$ as a function of $\phi_2/(\phi_1 + \phi_2)$, which represents the percentage of the total volume fraction occupied by the larger crowders. The level of stabilization decreases as the content of the larger crowders increases, echoing the finding in Fig. 4 that the larger crowders are less effective in stabilization than the smaller crowders.

An important question is whether the stabilization effect of the mixture is additive of the separate effects of the constituents. As an example, let $\Delta\Delta G_m$ be the change in folding stability by a mixture of the smaller and larger crowders, respectively occupying 15% and 20% of the total volume. Now let $\Delta\Delta G_1$ be the change in folding stability by the smaller crowders alone at a volume fraction of 15%, and $\Delta\Delta G_2$ be the counterpart for the larger crowders alone at a volume fraction of 20%. Is $\Delta\Delta G_m$ predicted well by adding $\Delta\Delta G_1$ and $\Delta\Delta G_2$? Because the fit to Eq. 4 worked so well for crowders with a single size, we simply used the fit to generate $\Delta\Delta G_f$ for the smaller or the larger crowders alone at desired volume fractions. Upon pairing the respective volume fractions to yield a total of 35%, the levels of stabilization due to the two types of crowders alone were added and the results are displayed in Fig. 5. It can be seen that the levels of stabilization produced by mixtures of the two types of crowders are greater than predicted by additivity.

Binding stability under crowding

Because two protein molecules become more compact when they form a complex, crowding is expected to stabilize the bound state (14). In this study, we used barnase and barstar as a test system. Fig. 6 displays the changes in binding free energy by crowders at four sizes (R_c from 15 to 50 Å) and at four volume fractions (ϕ from 5% to 35%). The trends observed here are very similar to those displayed in Fig. 3 for protein folding stability. The maximal increase in binding free energy, produced by crowders with a radius of 15 Å and occupying 35% of volume, was 3.2 k_BT, or 1.9 kcal/mol at room temperature.

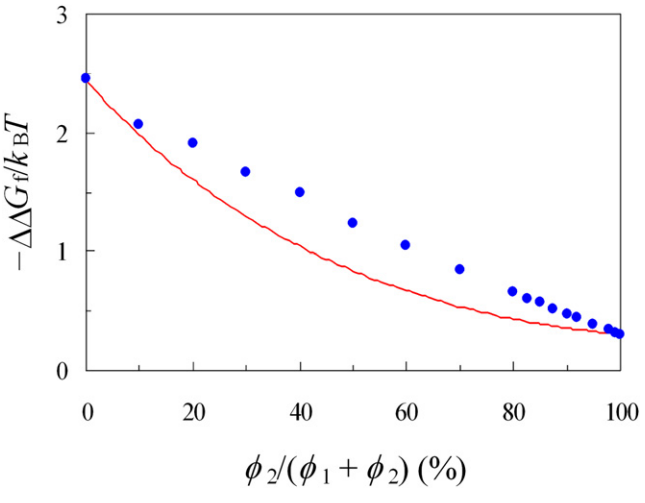

FIGURE 5 Increase in folding stability of cytochrome b_{562} by mixtures of crowders with 15 and 50 Å radii. Circles show the actual results for $\Delta\Delta G_f$ obtained from atomistic modeling; the curve shows additive prediction.

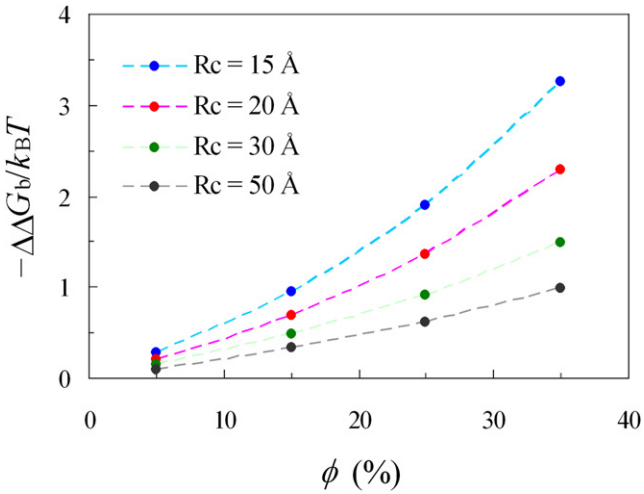

FIGURE 6 Dependence of $\Delta\Delta G_b$ on crowder radius R_c and volume fraction ϕ.

DISCUSSION

The magnitude of crowding-induced stabilization

The modest stabilization obtained in this study, based on atomistic modeling of macromolecular crowding, is in line with experimental measurements of crowding effects on protein folding stability (10–13). The maximal levels of stabilization observed in these experimental studies, using dextran, Ficoll, or polyethylene glycol as a crowding agent, were ~1 kcal/mol. Interestingly, simulations based on a coarse-grained model also yielded similarly modest stabilization by crowding (8,9). On the other hand, simple theoretical models, depending on how the denatured state is represented, have either predicted modest (5) or substantial (6) stabilization, indicating that these models are of limited value at a quantitative level.

The modest level of stabilization, of ~1 kcal/mol, can nevertheless be of physiological importance. In particular, in protein aggregation the modest stabilization of individual folding and binding equilibria can accumulate into significant stabilization of the nucleus for aggregation, resulting in considerable reduction in the lag time of aggregation. As illustrated in Fig. 7, a nucleus consisting of four monomers involve four folding events and three bimolecular binding events. If crowding favors each equilibrium in the forward direction by 1 kcal/mol, cumulatively, the stability of the nucleus (relative to the unfolded and unbound monomers) will be enhanced by 7 kcal/mol. This stabilization may explain the shortening of aggregation lag time from months to days observed for α-synuclein by the addition of crowding agents (23,24). Aggregation of this natively unfolded protein is implicated in Parkinson's disease.

The influence of crowder size on the level of stabilization

Our calculation results show that, when present at the same volume fraction, crowders with different sizes can lead to different levels of increase in protein folding and binding stability. This finding suggests that different crowding agents, when present at the same concentration, will produce different levels of stabilization.

This study only explored the variation in crowder size. Another important variable is crowder shape. When crowders differing in both shape and size are compared, one can only expect greater variation in the level of stabilization. Such variations in level of stabilization have been observed in an experimental study in which the effects of dextran species with different sizes and Ficoll were compared (25).

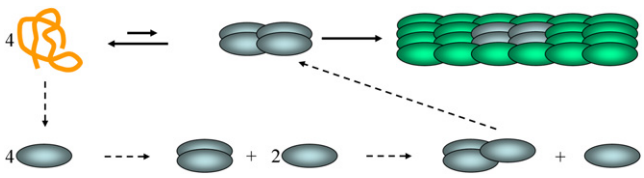

FIGURE 7 Illustration of a protein aggregation process. (*Top row*) Four unfolded monomers slowly form a nucleus; thereafter aggregation proceeds quickly. (*Bottom row*) The free-energy difference between the nucleus and the four unfolded monomers can be reconstructed sequentially, first forming four folded monomers and then adding monomers one at a time.

Nonadditive effects of mixed crowding

We found that the effect of a mixture of two types of crowders on protein folding stability is greater than the sum of the effects of the constituents. This nonadditive behavior has also been observed in an experimental study using dextran and Ficoll as mixed crowding agents (25). The nonadditivity can be viewed as a manifestation of the nonlinear dependence of the crowding-induced change in chemical potential on crowder concentrations (see Eq. 4 and Fig. 4). In particular, Fig. 4 shows that the $-\Delta\Delta G_f$ function curves upward as ϕ increases, The upward curving explains why the effect of mixed crowding, insofar as volume exclusion is concerned, is greater than predicted by additivity, The fact that this nonadditive behavior is precisely what is observed on mixtures of dextran and Ficoll (25) is strong evidence that volume exclusion plays an important role in the effects of these crowding agents on folding stability.

Since the cytosol is crowded by many species of macromolecules, the nonadditive effects of mixed crowding have important implications. First, they suggest that future studies should be directed at more-complex mixtures of crowding agents to realistically mimic cellular environments. Second, they identify composition as another important variable in controlling the effects of crowding. Together, crowder shape, size, composition, and concentration may inject significant variability in the effects of crowding on biophysical properties of proteins. It is known that abnormal (e.g., misfolded) proteins accumulate with age inside cells because of impairment of the cellular degradation machinery. The accumulation may lead to enhanced crowding effects, which in turn may explain why susceptibility to aggregation-related diseases such as Parkinson's disease increases with age.

Extensions and other applications

The subtle dependences on crowder species, concentration, and concentration make quantitative prediction of crowding effects a formidable challenge. The approach introduced in this study is well suited to meet this challenge. In our approach, simulations of test proteins and crowders are separated. The tasks for test proteins and for crowders are very different. For test proteins, the main interest is in sampling internal conformations; for crowders, the main interest is in generating an equilibrium distribution of crowder positions and orientations. The protein simulations require short time steps; without the encumbrance of crowders, relatively long simulations can be afforded. The crowder simulations can be accomplished by running Brownian dynamics simulations with relatively large time steps (26).

We have developed an efficient algorithm for calculating the increase in chemical potential of a test protein due to volume exclusion by crowders. Like other simulation studies of crowding and confinement (8,9,15,27,28), here we only considered a simple, spherical representation of crowders. In future work we will extend the approach to model crowders with atomic details and to account for other types of interactions between a test protein and crowders. These extensions will allow us to directly compare calculation results with experimental data.

Here our approach to the modeling of macromolecular crowding was applied to protein folding and binding equilibria. There are many other potential applications. For example, the biological functions of many proteins (or protein complexes) involve different conformational states; crowding may affect their equilibria. Minh et al. (15) have simulated the opening and closing of the flaps of an HIV-1 protease dimer in the presence of crowders. Our approach can be applied to reanalyze the many published simulations of conformational transitions carried out in the absence of crowding to find how crowding affects the results.

The approach works not only for equilibrium but also for kinetic properties. For example, when applied to the reactant and transition states, the effect of crowding on the activation barrier can be obtained. For the binding of proteins, we have developed a transient-complex theory, which predicts the rate constant as (29,30)

$$k_a = k_{a0} \exp(-\Delta U_{l\text{-}r} * / k_B T), \quad (5)$$

where $U_{l\text{-}r}$* is the interaction energy, due to long-range forces, in the transient complex for protein binding, and k_{a0} is the binding rate constant in the absence of any force. In the absence of crowding, $U_{l\text{-}r}$* comes from electrostatic interactions between the binding molecules. Crowding induces an effective interaction potential; its effect on k_a depends on whether it is long-ranged, i.e., with magnitude decreasing slowly as the binding molecules are moved apart. If the effective potential is short-ranged, then its effect on k_a is minimal (31). On the other hand, if the effective potential turns out to be long-ranged, its effect on the binding rate can be accounted for by including it as an additive contribution in calculating $U_{l\text{-}r}$* (5).

This work was supported in part by National Institutes of Health grant No. GM058187.

REFERENCES

1. Zimmerman, S. B., and S. O. Trach. 1991. Estimation of macromolecule concentrations and excluded volume effects for the cytoplasm of *Escherichia coli*. *J. Mol. Biol.* 222:599–620.
2. Minton, A. P. 1983. The effect of volume occupancy upon the thermodynamic activity of proteins: some biochemical consequences. *Mol. Cell. Biochem.* 55:119–140.
3. Minton, A. P. 2000. Effect of a concentrated "inert" macromolecular cosolute on the stability of a globular protein with respect to denaturation by heat and by chaotropes: a statistical-thermodynamic model. *Biophys. J.* 78:101–109.
4. Zhou, H.-X., and K. A. Dill. 2001. Stabilization of proteins in confined spaces. *Biochemistry.* 40:11289–11293.
5. Zhou, H.-X. 2004. Protein folding and binding in confined spaces and in crowded solutions. *J. Mol. Recognit.* 17:368–375.
6. Minton, A. P. 2005. Models for excluded volume interaction between an unfolded protein and rigid macromolecular cosolutes: macromolecular crowding and protein stability revisited. *Biophys. J.* 88:971–985.
7. Zhou, H.-X. 2008. Effect of mixed macromolecular crowding agents on protein folding. *Proteins.* 72:1109–1113.
8. Cheung, M. S., D. Klimov, and D. Thirumalai. 2005. Molecular crowding enhances native state stability and refolding rates of globular proteins. *Proc. Natl. Acad. Sci. USA.* 102:4753–4758.
9. Stagg, L., S. Q. Zhang, M. S. Cheung, and P. Wittung-Stafshede. 2007. Molecular crowding enhances native structure and stability of α/β protein flavodoxin. *Proc. Natl. Acad. Sci. USA.* 104:18976–18981.
10. Qu, Y., and D. W. Bolen. 2002. Efficacy of macromolecular crowding in forcing proteins to fold. *Biophys. Chem.* 101–102:155–165.
11. Spencer, D. S., K. Xu, T. M. Logan, and H.-X. Zhou. 2005. Effects of pH, salt, and macromolecular crowding on the stability of FK506-binding protein: an integrated experimental and theoretical study. *J. Mol. Biol.* 351:219–232.
12. Ai, X., Z. Zhou, Y. Bai, and W. Y. Choy. 2006. ^{15}N NMR spin relaxation dispersion study of the molecular crowding effects on protein folding under native conditions. *J. Am. Chem. Soc.* 128:3916–3917.
13. Roberts, A., and S. E. Jackson. 2007. Destabilized mutants of ubiquitin gain equal stability in crowded solutions. *Biophys. Chem.* 128:140–149.
14. Zhou, H.-X., G. Rivas, and A. P. Minton. 2008. Macromolecular crowding and confinement: biochemical, biophysical, and potential physiological consequences. *Annu. Rev. Biophys.* 37:375–397.
15. Minh, D. D., C. E. Chang, J. Trylska, V. Tozzini, and J. A. McCammon. 2006. The influence of macromolecular crowding on HIV-1 protease internal dynamics. *J. Am. Chem. Soc.* 128:6006–6007.
16. Widom, B. 1963. Some topics in the theory of fluids. *J. Chem. Phys.* 39:2802–2812.
17. Huang, X., and H.-X. Zhou. 2006. Similarity and difference in the unfolding of thermophilic and mesophilic cold shock proteins studied by molecular dynamics simulations. *Biophys. J.* 91:2451–2463.
18. Tjong, H., and H.-X. Zhou. 2008. Accurate calculations of binding, folding, and transfer free energies by a scaled generalized Born method. *J. Chem. Theory Comput.* 4:1733–1744.
19. Zhou, H.-X., and A. Szabo. 1991. Comparison between molecular dynamics simulations and the Smoluchowski theory of reactions in a hard sphere liquid. *J. Chem. Phys.* 95:5948–5952.
20. Allen, M. P., and D. J. Tildesley. 1987. Computer Simulation of Liquids. Clarendon Press, Oxford, UK.
21. Bondi, A. 1964. van der Waals volumes and radii. *J. Phys. Chem. B.* 68:441–451.
22. Lebowitz, J. L., and J. S. Rowlinson. 1964. Thermodynamic properties of mixtures of hard spheres. *J. Chem. Phys.* 41:133–138.
23. Shtilerman, M. D., T. T. Ding, and P. T. Lansbury, Jr. 2002. Molecular crowding accelerates fibrilization of α-synuclein: could an increase in the cytoplasmic protein concentration induce Parkinson's disease? *Biochemistry.* 41:3855–3860.
24. Uversky, V. N., M. Cooper, K. S. Bower, J. Li, and A. L. Fink. 2002. Accelerated α-synuclein fibrillation in crowded milieu. *FEBS Lett.* 515:99–103.
25. Batra, J., K. Xu, and H.-X. Zhou. 2009. Nonaddtive effects of mixed crowding on protein stability. *Proteins.* In press.

26. McGuffee, S. R., and A. H. Elcock. 2006. Atomically detailed simulations of concentrated protein solutions: the effects of salt, pH, point mutations, and protein concentration in simulations of 1000-molecule systems. *J. Am. Chem. Soc.* 128:12098–12110.

27. Takagi, F., N. Koga, and S. Takada. 2003. How protein thermodynamics and folding mechanisms are altered by the chaperonin cage: molecular simulations. *Proc. Natl. Acad. Sci. USA.* 100:11367–11372.

28. Mittal, J., and R. B. Best. 2008. Thermodynamics and kinetics of protein folding under confinement. *Proc. Natl. Acad. Sci. USA.* 105:20233–20238.

29. Alsallaq, R., and H.-X. Zhou. 2007. Energy landscape and transition state of protein-protein association. *Biophys. J.* 92:1486–1502.

30. Alsallaq, R., and H.-X. Zhou. 2008. Electrostatic rate enhancement and transient complex of protein-protein association. *Proteins.* 71:320–335.

31. Schreiber, G., G. Haran, and H.-X. Zhou. 2009. Fundamental aspects of protein-protein association kinetics. *Chem. Rev.* 109:839–860.